Electronic Supplementary Material (ESI) for Sustainable Energy & Fuels.

Hematite Photoanodes Prepared by Particle Transfer for Photoelectrochemical Water Splitting

Zhenhua Pan,[1*] Rito Yanagi,[2,3] Tomohiro Higashi,[4] Yuriy Pihosh,[5] Shu Hu,[2,3] Kenji Katayama[1]

[1] Department of Applied Chemistry, Faculty of Science and Technology, Chuo University, 1-13-27 Kasuga, Bunkyo, Tokyo 112-8551, Japan

[2] Department of Chemical and Environmental Engineering, School of Engineering and Applied Sciences, Yale University, New Haven, CT 06520, USA.

[3] Energy Sciences Institute, Yale West Campus, West Haven, CT 06516, USA.

[4] Institute for Tenure Track Promotion, University of Miyazaki, Nishi 1-1 Gakuen-Kibanadai, Miyazaki 889-2192, Japan

[5] University Professors Office, The University of Tokyo, Bunkyo-ku, Tokyo 113-8656, Japan

*Corresponding Author: zhenhua.20y@g.chuo-u.ac.jp

S1 Experimental section

Preparation of thin-film α-Fe_2O_3 photoanodes. Thin-film α-Fe_2O_3 was coated on a fluorine-doped tin oxide (FTO) quartz substrate (~ 7 Ω sq^{-1}, Solaronix) by a solution-derived method as shown in Figure S1 following a previous study.[1] First, β-FeOOH was grown on FTO in a solution containing 0.15 M iron (III) chloride hexahydrate ($FeCl_3$, Wako Pure Chemical Industries. Ltd., 99.9%) and 1 M sodium nitrate ($NaNO_3$, Wako Pure Chemical Industries. Ltd., 99.9%) at 100 °C for 2 h. Then, β-FeOOH on FTO was annealed at 500, 600, 700, 800, or 900 °C for 2 h to obtain thin-film α-Fe_2O_3 on FTO. Finally, thin-film α-Fe_2O_3 on FTO was connected with a lead wire using indium and used as a photoanode.

Preparation of α-Fe_2O_3 particles. α-Fe_2O_3 particles were prepared by a solution-derived method as shown in Figure S3. First, a 100 mL solution containing 0.15 M iron (III) chloride hexahydrate ($FeCl_3$, Wako Pure Chemical Industries. Ltd., 99.9%) and 1 M sodium nitrate ($NaNO_3$, Wako Pure Chemical Industries. Ltd., 99.9%) was subjected to a thermal treatment at 100 °C for 2 h to obtain β-FeOOH suspension. The β-FeOOH suspension was filtrated, washed with sufficient deionized water, and dried at 80 °C overnight. The obtained particles were annealed at 500, 600, 700, 800, or 900 °C for 2 h to prepare α-Fe_2O_3 particles. For preparing Sn-doped α-Fe_2O_3 particles, Tin(IV) chloride pentahydrate (1 mol% of Fe, $SnCl_4 \cdot 5H_2O$, FUJIFILM Wako Pure Chemical Corporation, 98.0%) was added to the precursor solution of β-FeOOH and other procedures were the same as those for α-Fe_2O_3 particles.

Preparation of particulate α-Fe_2O_3 photoanodes. Particulate α-Fe_2O_3 photoanodes were fabricated through a particle-transfer method as shown in Figure S4.[2] Briefly, ~ 10 mg α-Fe_2O_3 particles were suspended in a 450 μL isopropanol solution by sonication. The suspension of 30 μL was drop-casted on a 1 cm × 3 cm glass substrate three times. After the drop-cast glass substrate was fully dried in the air, a conductive layer of Ti with a thickness of aprox. 2.5 μm was deposited on the α-Fe_2O_3 particles by an electron-beam evaporation (ULVAC, CV-S) to form an ohmic contact with α-Fe_2O_3 particles. Another glass substrate with a conductive carbon tape was used to attach and peel off the Ti film. The transferred Ti

film conjugated with α-Fe_2O_3 particles was sonicated in water for 10 s to remove the excessive particles without a direct contact with the Ti film. Finally, the Ti film was connected with a lead wire using indium solder and unused region was covered by epoxy resin for insulation. The obtained assembly of α-Fe_2O_3/Ti/glass substrates were used as photoanodes.

Deposition of cocatalysts on photoanodes. CoP_i was loaded by photoelectrochemical deposition in a 0.1 M KPi buffer solution containing 0.5 mM $Co(NO_3)_3$ at pH = 7.2 under simulated sunlight illumination (PEL-L01, PECCELL, AM 1.5G, 100 mW cm^{-2}) at a potential of 1.05 V_{RHE} for 5 min.

CoO_x, $FeNiO_x$ and $CoFeNiO_x$ cocatalysts were loaded on α-Fe_2O_3 photoanodes by a dipping method. For loading CoO_x, a Co-based solution was firstly prepared by mixing cobalt (II) 2-ethylhexanoate (20 μL, Wako) with hexane (10 mL, HPLC grade, Wako). The α-Fe_2O_3 photoanode was dipped into the Co-based solution for 10 s and then dried in the air naturally. Finally, the photoanode was annealed in air at 140 ˚C for 45 minutes. For loading $FeNiO_x$, a FeNi-complex solution was firstly prepared by mixing iron (III) 2-ethylhexanoate (10 μL, Wako), nickel (II) 2-ethylhexanoate (10 μL, Wako), and hexane (10 mL, HPLC grade, Wako). The α-Fe_2O_3 photoanode was dipped into the FeNi-complex solution for 20 s and then dried in the air naturally. Finally, the photoanode was annealed in air at 140 ˚C for 45 minutes. For loading $CoFeNiO_x$, a Co-based solution and a FeNi-complex solution were prepared as mentioned above. The α-Fe_2O_3 photoanode was dipped into the FeNi-complex solution for 10 s, dried in the air, then dipped into Co-based solution for 5 s, and again dried naturally in the air. This dipping process was repeated twice. Finally, the photoanode was annealed in air at 140 ˚C for 45 minutes.

A $NiCoFeBO_x$ cocatalyst was loaded on α-Fe_2O_3 photoanodes by a photoelectrochemical deposition method, following a previous study.[3] A standard three-electrode system was employed for the deposition, where the α-Fe_2O_3 photoanode, a Ag/AgCl electrode, and a Pt wire were used as the working, reference, and counter electrodes. They electrolyte was a $K_2B_4O_7 \cdot 4H_2O$ buffer solution (0.25 M, pH = 10, 99.99% trace metals basis, Sigma Aldrich) containing $NiSO_4 \cdot 6H_2O$ (2 mM, 99.99% trace metals basis, Sigma Aldrich), $Co(NO_3)_2 \cdot 6H_2O$

(0.5 mM, 99.99% trace metals basis, Sigma Aldrich) and $FeSO_4 \cdot 7H_2O$ (0.8 mM, 99.99% trace metals basis, Sigma Aldrich). Before deposition, the freshly made solution was stirred and bubbled by N_2 gas for ~ 25 min. Then the photoelectrochemical deposition was conducted at a current density of 10 μA cm^{-2} under AM1.5G simulated solar light for 10 min. After photo-electrodeposition, the electrode was washed with deionized water and dried by N_2.

Photoelectrochemical (PEC) and electrochemical impedance spectroscopy measurement. The PEC activities of photoanodes were measured by a three-electrode electrochemical configuration in 0.1 M KPi buffer solution at pH = 7.2 under simulated sunlight illumination (PEL-L01, PECCELL, AM 1.5G, 100 mW cm^{-2}). Before the measurement, the electrolyte was purged with N_2 gas for 20 min. The electrolyte was stirred and bubbled with N_2 gas during measurement. An Ag/AgCl electrode in saturated KCl solution (0.198 V vs. NHE) and a Pt wire were used as the reference and counter electrodes, respectively. The potential of the working electrode was controlled by a potentiostat (ALS/CH Instruments, Model 660A) with a scan rate of 10 mV s^{-1}. Onset potential (E_{on}) is defined as the starting potential where the currents in dark and under illumination show a difference of 0.01 mA cm^{-2}. Electrochemical impedance spectroscopy measurements were performed in the same three-electrode electrochemical configuration for obtaining the Mott-Schottky (without illumination) and Nyquist plots (under illumination).

IPCE measurements. The incident photon-to-current conversion efficiency (IPCE) was measured using a MAX-302 Xe light source (Asahi Spectra, Japan) equipped with bandpass filters to provide monochromatic light. Values of the IPCE were obtained by the following equation:

$$IPCE\ (\%) = \left[\left(\frac{1240}{\lambda} \right) \times \frac{J}{P} \right] \times 100,$$

where λ (nm) is the wavelength of the monochromatic incident light, J (mA cm^{-2}) is the photocurrent density at 1.23 V_{RHE} and P (mW cm^{-2}) is the power density of the incident light.

Characterization. The X-ray diffraction (XRD) pattern was recorded with a Rigaku SmartLab diffractometer with Cu Kα radiation, operating at 40 kV and 30 mA. The light absorption spectrum was obtained by a UV-visible-near infrared diffuse-reflectance spectroscopy (DRS, V-670, JASCO). The Scanning electron microscope (SEM) images were taken by scanning electron microscopy (Hitachi SU8020).

Parallel PEC cell. A PEC cell with a parallel configuration (parallel PEC cell) was constructed by connecting a Ga-doped LTCA (Ga-LTCA)-based particulate photocathode prepared through a particle transfer method[4, 5] and a particulate α-Fe_2O_3 photoanode. Prior to fabricating the parallel PEC cell, surface modifications for the photoelectrodes of Ga-LTCA and α-Fe_2O_3 were conducted. For the Ga-LTCA photocathodes, surface protective layer of TiO_2 was deposited on the Ga-LTCA surface, subsequently loading of Pt cocatalyst for promoting H_2 evolution reaction following the previously reported protocol.[3] For the α-Fe_2O_3 photoanodes, CoP_i cocatalysts for O_2 evolution reaction were loaded on the surface by photoelectrochemical deposition as mentioned before. Both surface-modified photoelectrodes were mounted side by side on a glass plate. The PEC water splitting reaction was conducted in 0.1 M KP_i buffered aqueous solution (pH = 7.2) in an airtight reactor with a flat window and a cooling jacket. The reactor was purged with Ar gas and maintained at atmospheric pressure. The cell was irradiated by a simulated AM1.5G light (XES-70S1, San-ei electronic). The photocurrent was recorded as the chronoamperogram in the two-electrode configuration without applying an external bias voltage. The quantities of evolved hydrogen and oxygen were determined using a micro gas chromatograph (Model 3000, Inficon Co. Ltd.)

Solar-to-hydrogen energy conversion efficiency (STH) of the parallel PEC cell composted of the α-Fe_2O_3 photoanode and the Ga-LTCA photocathode was calculated from the *i-t* curve of the cell by the following equation:

$$STH(\%) = J \times 1.23\,V \times 100/\,P,$$

where J is the photocurrent density (mA cm^{-2}), and P is the power density of the incident light, AM1.5G solar simulator (100 mW cm^{-2}). The effective electrode area of the PEC cell was the total effective areas of the α-Fe_2O_3 photoanode and the Ga-LTCA photocathode used.

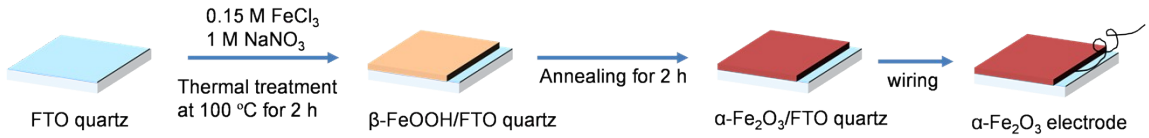

Figure S1 Preparation of a thin-film α-Fe_2O_3 electrode by a solution-derived method.

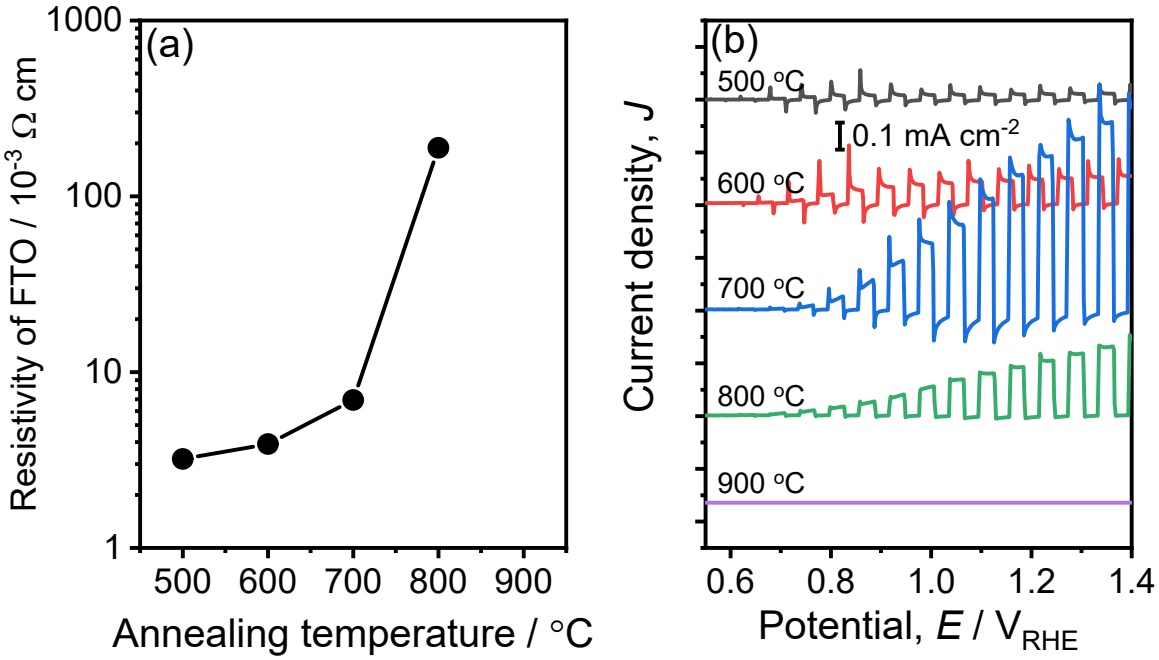

Figure S2 (a) The resistivities of FTO on quartz after annealing at various temperatures. The resistivity of FTO after annealing at 900 °C is higher than the detection limit. The thickness of FTO is 500 nm. (b) The PEC activities of CoP_i-loaded α-Fe_2O_3/FTO were obtained at various annealing temperatures. Electrolyte, 0.1 M phosphate buffer (pH 7.2); light source, solar simulator AM1.5G, 100 mW cm^{-2}. Thin-film α-Fe_2O_3 photoanodes with FTO quartz were fabricated at various annealing temperatures by a solution-derived method (Figure S1).

149 At above 700 °C, the electric conductivity of FTO significantly decreased (Figure S2a). Since
150 the electron transfer to the substrate was inhibited, the α-Fe_2O_3 photoanodes prepared at
151 above 800 °C showed poorer PEC performance than those prepared at lower temperatures
152 (Figure S2b), even though the former may exhibit superior optoelectronics for photocatalysis.
153
154

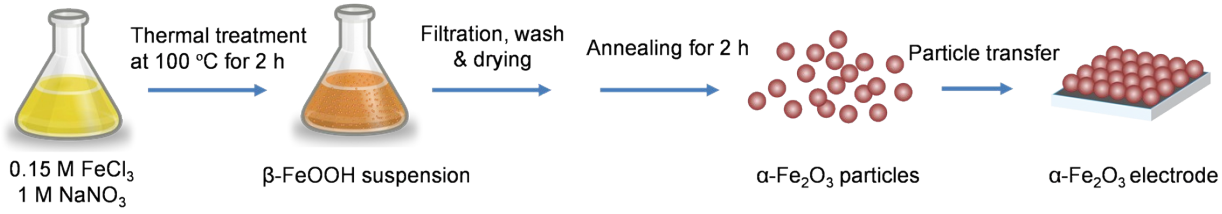

155
156 Figure S3 Fabrication of α-Fe_2O_3 particles by a solution-derived method.
157

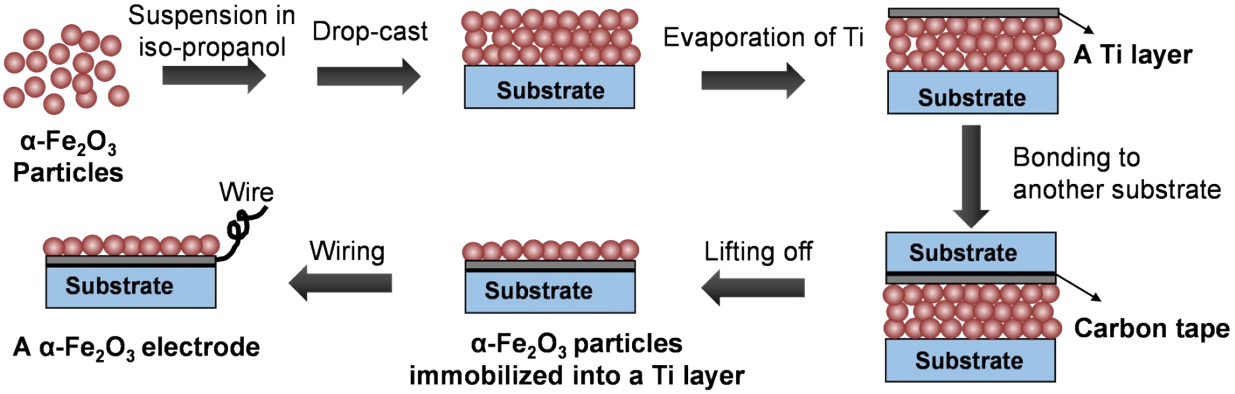

158
159 Figure S4 A particle-transfer method for fabricating a particulate α-Fe_2O_3 electrode.
160
161
162

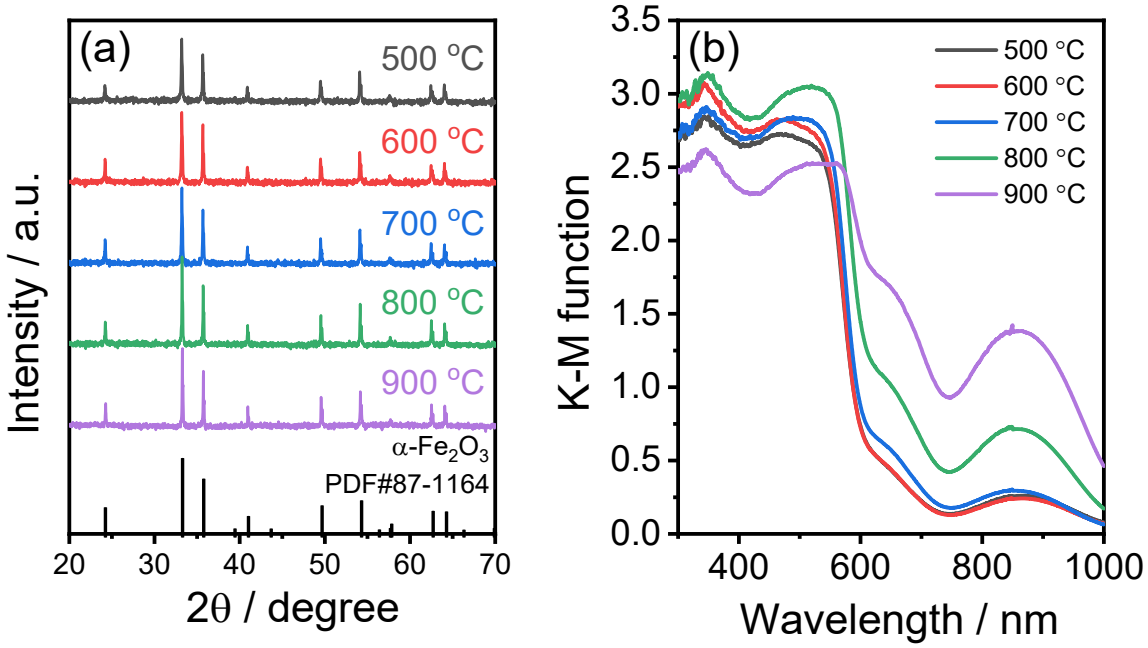

163

164 Figure S5 (a) XRD patterns and (b) DRS of α-Fe_2O_3 particles prepared at various annealing

165 temperatures.

166

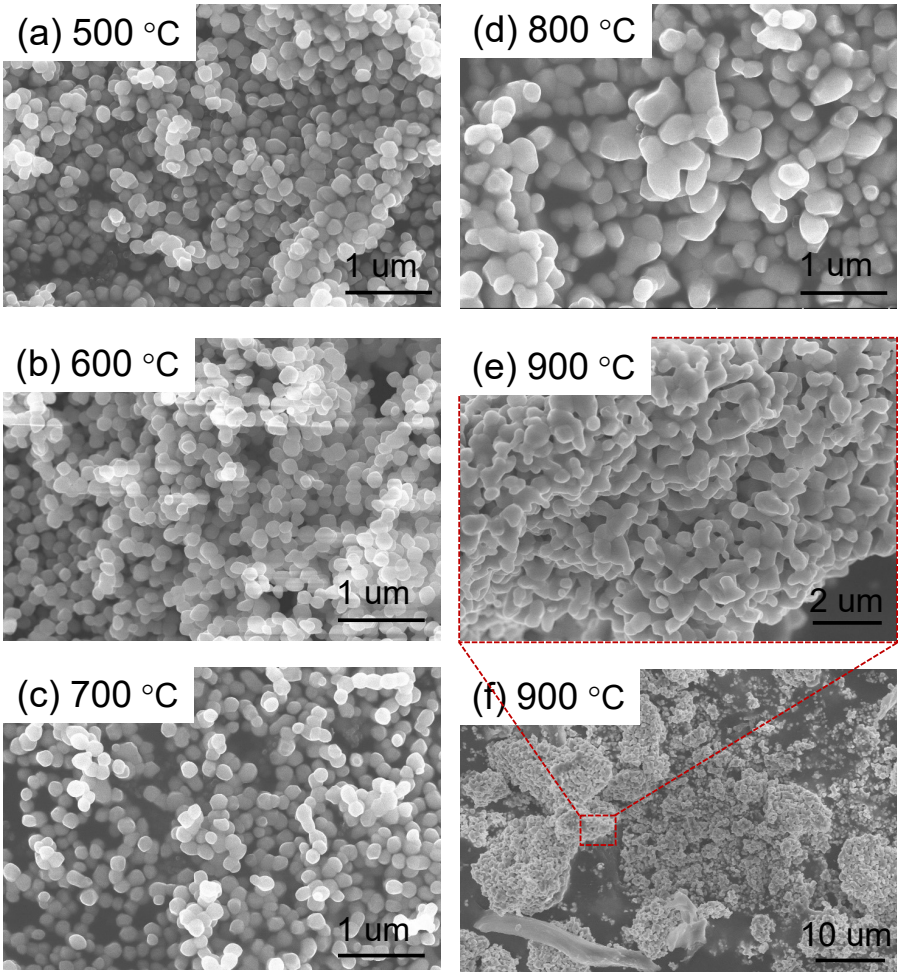

Figure S6 SEM images of α-Fe_2O_3 particles prepared at various annealing temperatures.

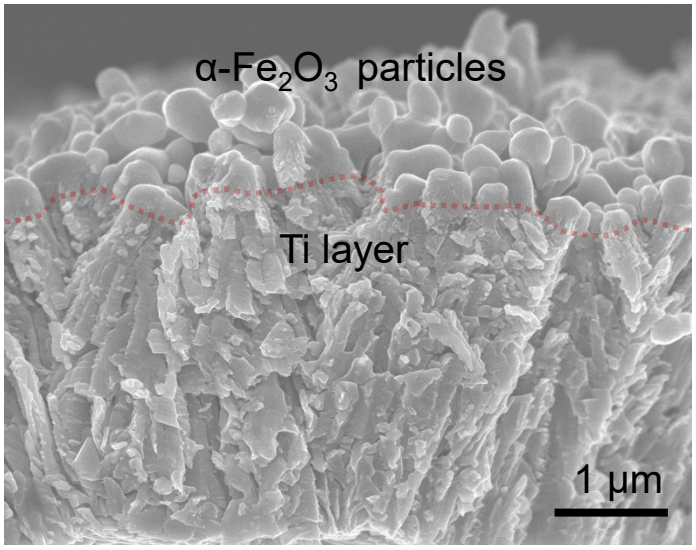

Figure S7 A SEM image of α-Fe_2O_3 particles immobilized on a Ti layer. The dotted line indicates the interface between α-Fe_2O_3 particles and the Ti layer.

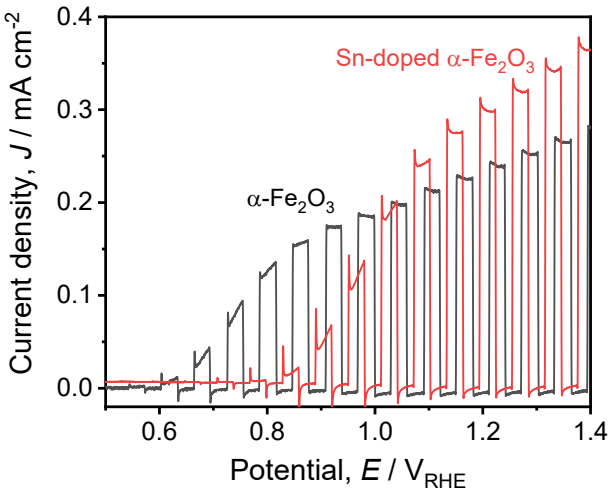

Figure S8 The PEC activities of α-Fe_2O_3(800 °C) and Sn-doped α-Fe_2O_3(800 °C) photoanodes. Cocatalyst, CoP_i loaded by photoelectrochemical deposition; electrolyte, 0.1 M phosphate buffer (pH 7.2); light source, solar simulator AM1.5G, 100 mW cm^{-2}.

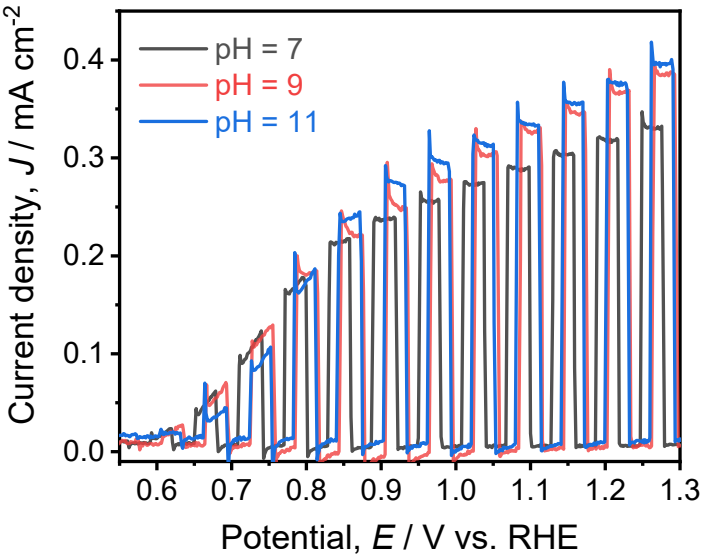

Figure S9 The PEC activities of a α-Fe_2O_3(800 °C) photoanode at pH 7, 9 and 11. Cocatalyst, CoP_i loaded by photoelectrochemical deposition; electrolyte, 0.1 M phosphate buffer (pH 7.2); light source, solar simulator AM1.5G, 100 mW cm^{-2}.

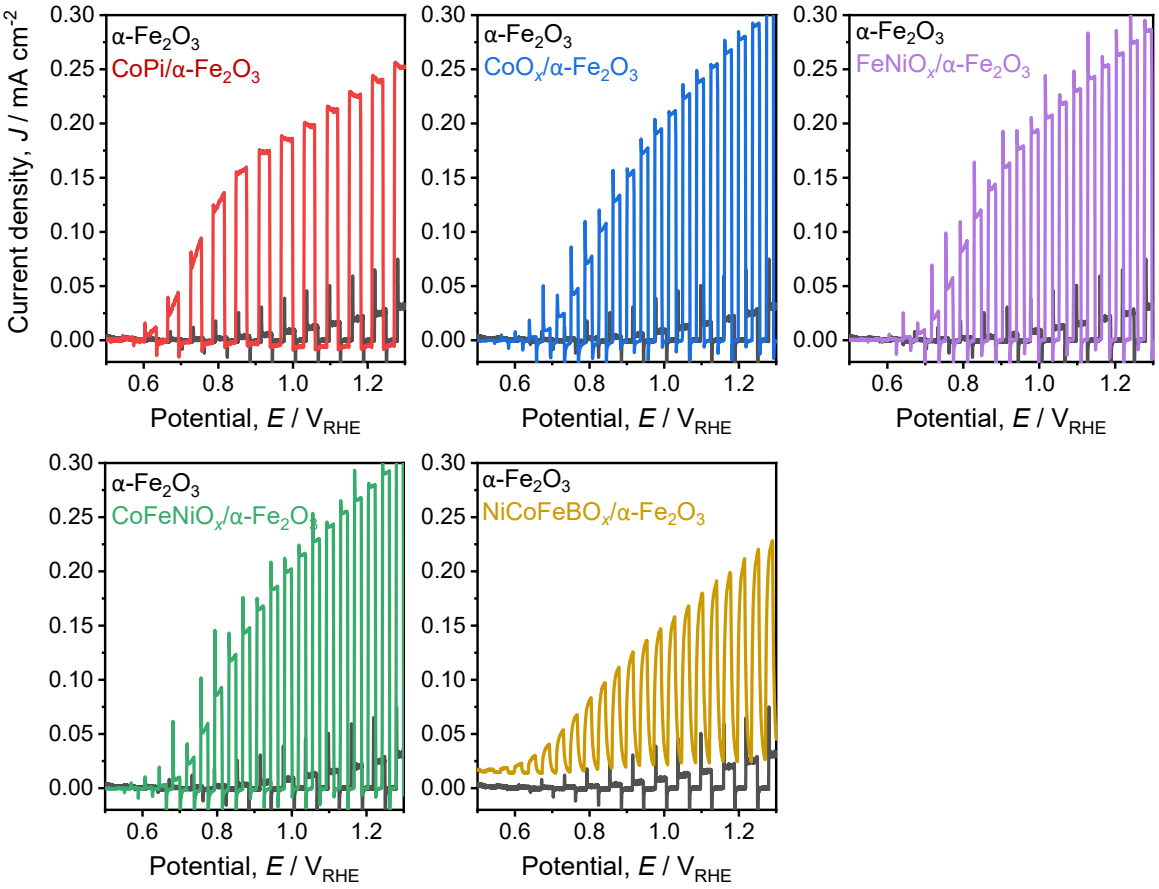

189

190 Figure S10 The PEC activities of α-Fe_2O_3(900 °C) photoanodes loaded with various
191 cocatalysts. Electrolyte, 0.1 M phosphate buffer (pH 7.2); light source, solar simulator
192 AM1.5G, 100 mW cm^{-2}.

193

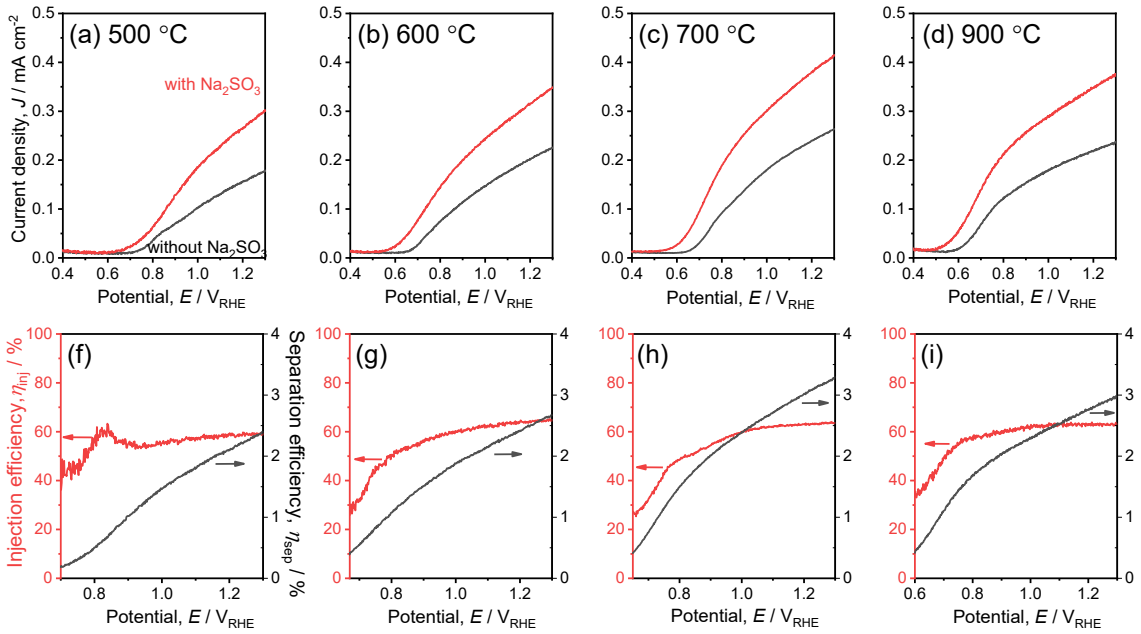

Figure S11 (a-d) The PEC activities of α-Fe_2O_3(500, 600, 700 and 900 °C) photoanodes with and without Na_2SO_3. (f-i) The η_{sep} and η_{inj} of α-Fe_2O_3(500, 600, 700 and 900 °C) photoanodes. Cocatalyst, CoP_i loaded by photoelectrochemical deposition; electrolyte, 0.1 M phosphate buffer (pH 7.2), if a hole scavenger is applied, with additional 0.2 M Na_2SO_3; light source, solar simulator AM1.5G, 100 mW cm^{-2}.

S2 Simulation section

S2.1 Optical simulation:

Optical simulation was carried out using COMSOL Multiphysics with a wave optics module. The overall model was set to be glass/water/hematite/Ti according to experimental conditions. The refractive index *n* for glass, water, and Ti were set to be 1.47, 1.33, and 2.6, respectively. The extinction coefficient *k* for glass, water, and Ti were set to be 0.

The thickness of the α-Fe_2O_3 layer was set to be 600 nm according to the main text. The refractive index $n(\lambda)$ and extinction coefficient $k(\lambda)$ of α-Fe_2O_3 are taken from literature and shown in Figure S12a.[6] The $n(\lambda)$ and $k(\lambda)$ of α-Fe_2O_3 serve as input in the simulation. The optical metrics consisting of absorption, reflection loss, and transmission loss were simulated based on this input and shown in Figure S12b.

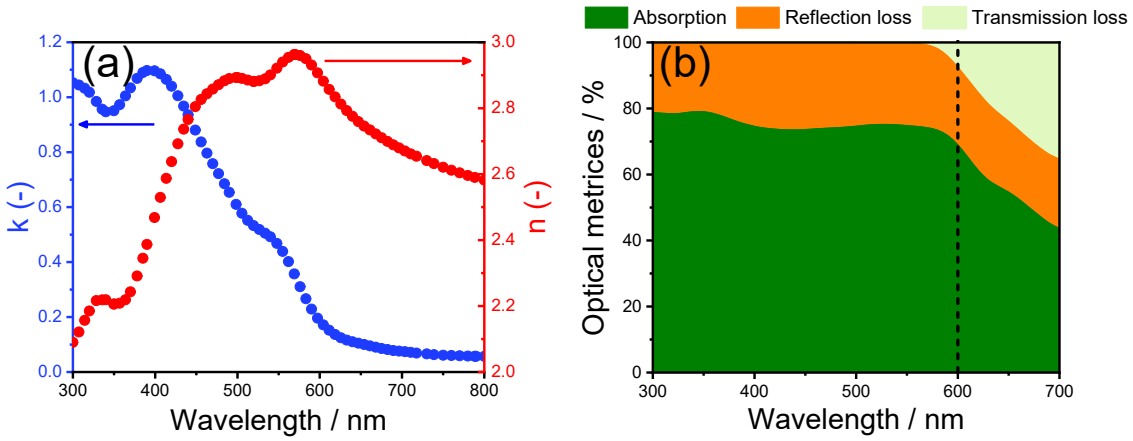

Figure S12 (a) The refractive index $n(\lambda)$ and extinction coefficient $k(\lambda)$ of α-Fe_2O_3. (b) Simulated optical metrics accounting for absorption, reflection loss, and transmission loss based on the $n(\lambda)$ and $k(\lambda)$.

S2.2 Generation rate calculation:

The AM1.5G solar spectrum is shown in Figure S13a. The energy of a single photon E is expressed as:

$$E = \frac{hc}{\lambda},$$

where h is Planck constant, c is speed of light, and λ is wavelength. Using this equation, the AM1.5G solar spectrum was converted to photon flux at electrode surface, $N_0(\lambda)$, as shown in Figure S13b. Subsequently, penetration depth (y) and wavelength (λ) dependent generation rate $G(y,\lambda)$ can be expressed as:

$$G(y,\lambda) = \alpha(\lambda) N_0(\lambda) e^{-\alpha(\lambda) y},$$

where $\alpha(\lambda)$ is the wavelength dependent absorption coefficient. Then $\alpha(\lambda)$ can be expressed using the extinction coefficient $k(\lambda)$ as follows:

$$\alpha(\lambda) = \frac{4\pi k(\lambda)}{\lambda}.$$

Therefore, $G(y,\lambda)$ can be expressed with $k(\lambda)$:

$$G(y,\lambda) = \frac{4\pi}{\lambda} k(\lambda) N_0(\lambda) e^{\frac{-4\pi}{\lambda} k(\lambda) y}.$$

Finally, the generation rate at a specific y, $G(y)$, is obtained by integrating over the wavelength up to the absorption edge of 600 nm. The calculated $G(y)$ profile is shown in Figure S13c.

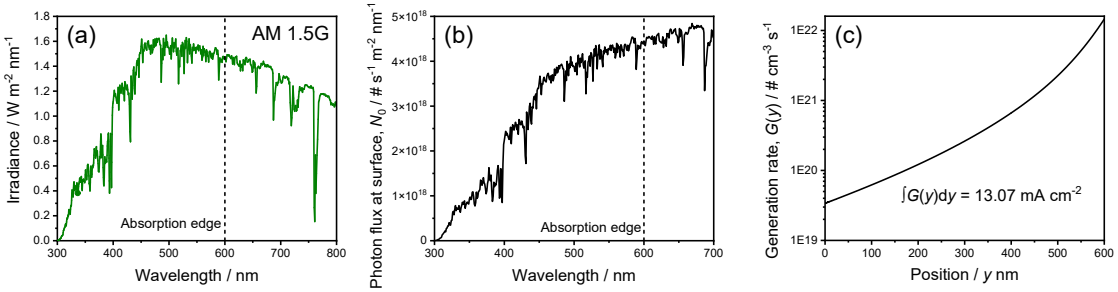

Figure S13 (a) AM 1.5G solar spectrum. (b) Photon flux at electrode surface. (c) Position-dependent generation rate.

S2.3 Electrical simulation:

Electrical simulation was carried out using COMSOL Multiphysics with a semiconductor module. The geometry was set to 1D and hematite was set to be 600 nm in thickness. Back contact was set to be an ideal ohmic contact, while the liquid contact was set to be a Schottky contact with varying built-in potentials. Potentials were applied to the hematite through the back contact. The applied potential E(V) was converted to the potential $E(\mathrm{V_{RHE}})$ scale using the following equation:

$$E(V_{RHE}) = 0.47 + E(V) \quad (1)$$

The charge-carrier generation rate was calculated based on the AM 1.5G solar spectrum and the absorption coefficient of α-Fe_2O_3, as described in the previous section. Recombination was modeled using trap-assisted Shockley-Read-Hall recombination with various carrier lifetimes.

To introduce a series resistance, the α-Fe_2O_3 photoanode was connected to a circuit using the AC/DC module of COMSOL. Ground, resistor, and a voltage source were introduced into the circuit as shown in Figure S15.

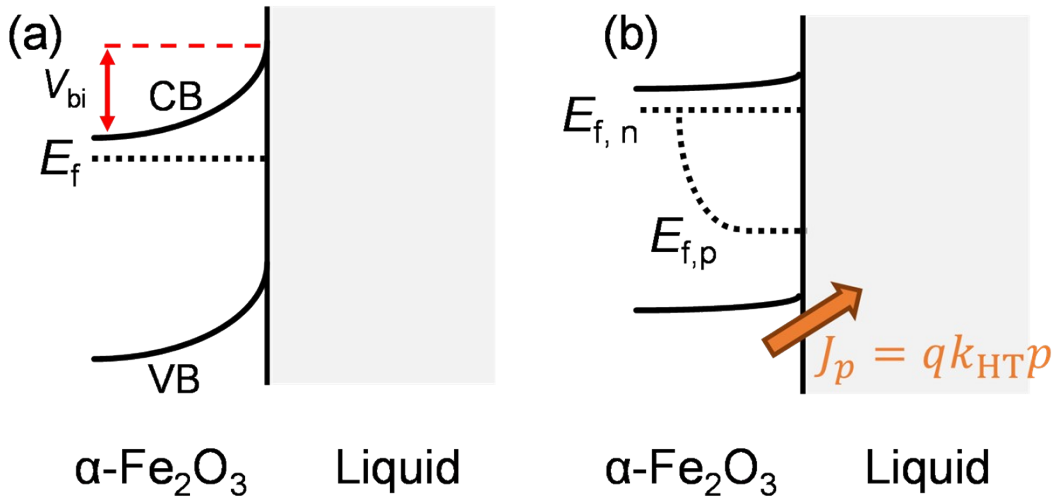

Figure S14 (a) The band energetics of a α-Fe_2O_3/liquid interface under equilibrium in the dark. V_{bi} is the built-in potential at the liquid interface under equilibrium; CB is conduction band; VB is valence band; E_f is the Fermi level of α-Fe_2O_3. (b) The band energetics of a α-

Fe_2O_3/liquid interface under equilibrium under illumination. $E_{f,\,n}$ and $E_{f,\,p}$ are the electron- and hole- quasi-Fermi level of α-Fe_2O_3, respectively; J_p is the hole current density from α-Fe_2O_3 to liquid; p is surface hole concentration; k_{HT} is hole transfer rate constant and is termed as "surface recombination velocity" in COMSOL software.

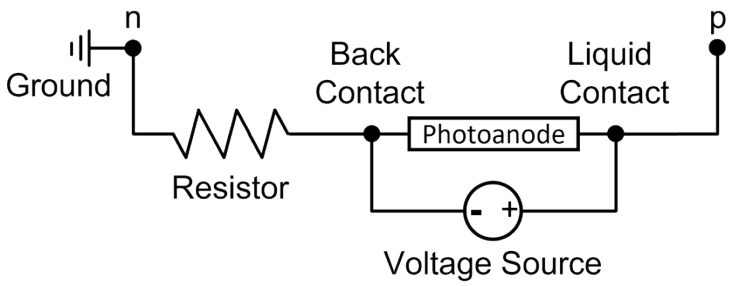

Figure S15. Settings for the AC/DC module according to the equivalent circuit.

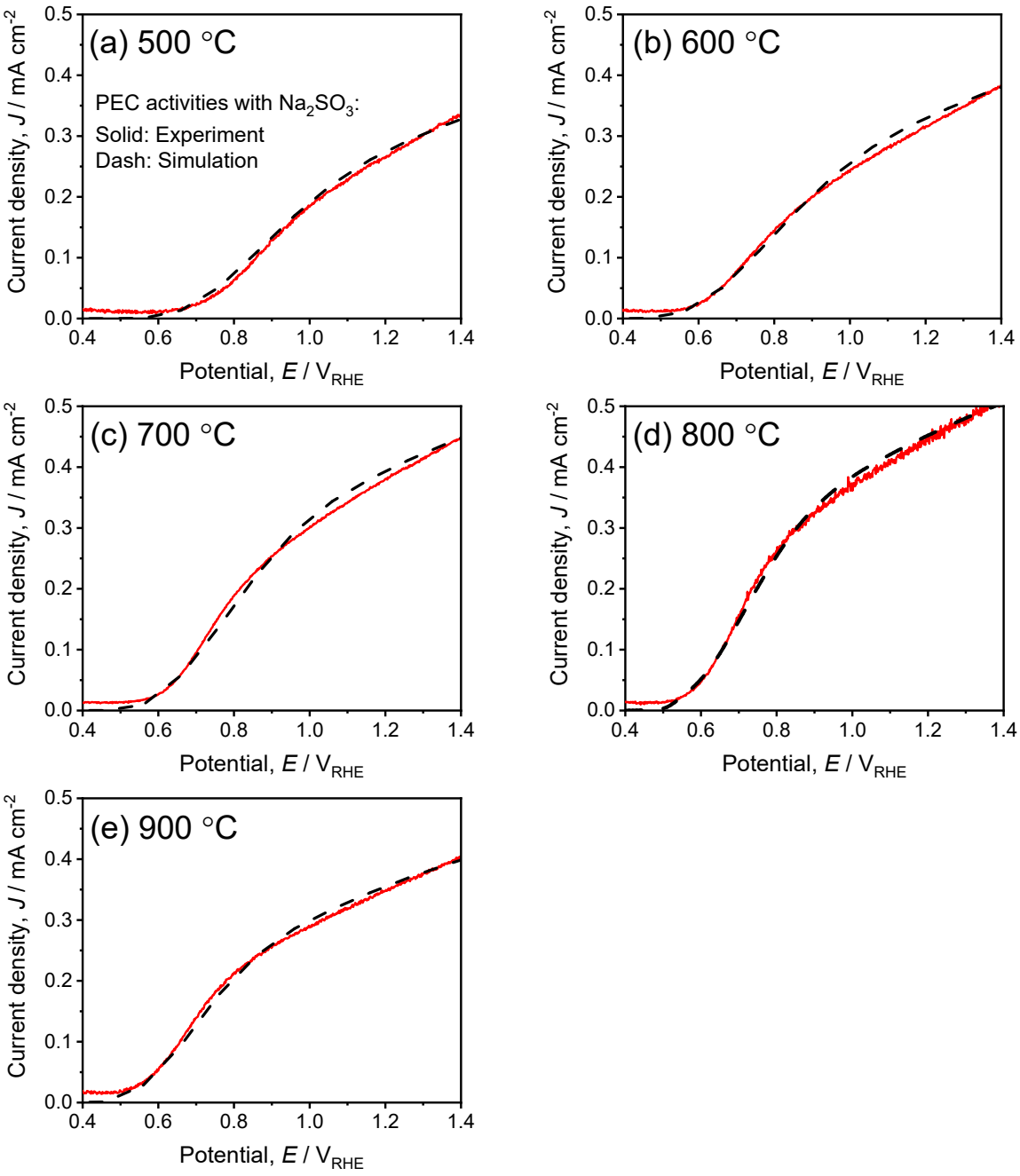

273

274 Figure S16 Experimental and simulated *J-E* curves of α-Fe_2O_3(500, 600, 700, 800 and 900

275 °C) photoanodes for sulfite oxidation.

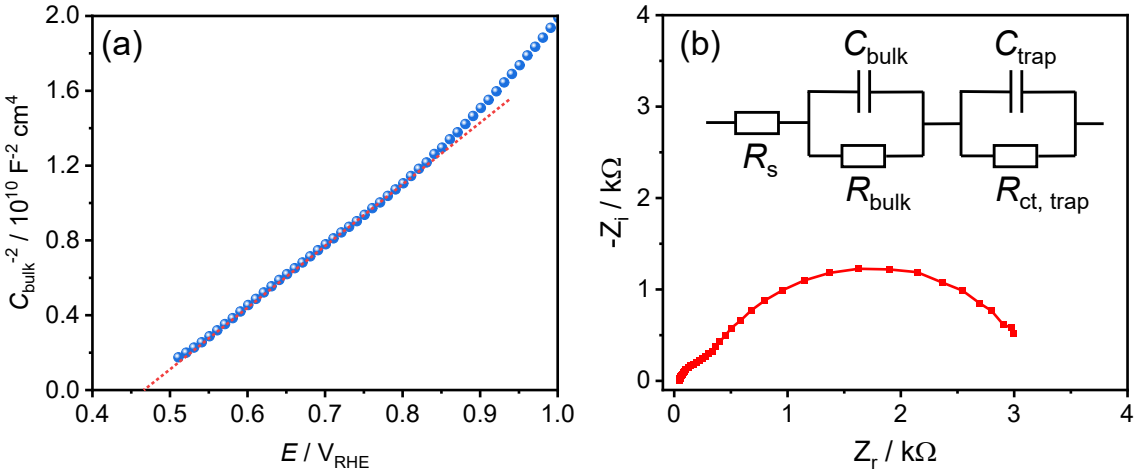

Figure S17 (a) Mott-Schottky plot for a α-Fe_2O_3 photoanode. The impedance spectra were recorded at a frequency of 1000 Hz. The *n*-type doping density of α-Fe_2O_3 was calculated from the slope of the plot and its value is 1×10^{20} cm^{-3}. (b) Nyquist plot of a CoP_i/α-Fe_2O_3 photoanode at 1.0 V_{RHE} under illumination and its equivalent circuit used for fitting. R_s, R_{bulk}, and $R_{ct, trap}$ represent the series resistance in the circuit, resistance for charge transfer in bulk and resistance for charge transfer from surface states across interface for O_2 evolution, respectively. By fitting, R_s, R_{bulk}, $R_{ct, trap}$ were confirmed to be 48, 414, and 2438 Ω, respectively. The series resistance applied to simulation in Figure 2d is equal to the sum of R_s and R_{bulk}. Note that the samples used for these measurements are thin-film α-Fe_2O_3 photoanodes rather than particulate α-Fe_2O_3 photoanodes since the rough surface of the latter will disturb the measurements. The thin-film α-Fe_2O_3 photoanodes were prepared at the same conditions as the particulate α-Fe_2O_3 photoanodes.

Table S1 Material parameters employed for electrical simulations

Parameters	Values
Energy band gap, E_g	2.1 eV
Conduction band minimum, E_c	0.3 V_{RHE}
Effective density of states for conduction and valence energy bands[a], $N_{c,v}$	10^{23} cm^{-3}
Flat band potential[b], E_{FB}	0.47 V_{RHE}
n-type doping density[b], N_d	1×10^{20} cm^{-3}
Dielectric constant[7], ε	32
Electron mobility[8], μ_n	0.01 cm^2 V^{-1} s^{-1}
Electrical conductivity[8], σ	10^{-14} $\Omega^{-1}cm^{-1}$
Hole diffusion length[8], L_D	4 nm

[a] $N_{c,v}$ was estimated based on E_c, E_{FB} and N_d.

[b] E_{FB} and N_d were extrapolated from Mott-Schottky plots in Figure S17a.

Table S2 Material parameters extracted from electrical simulations for α-Fe_2O_3 photoanodes prepared at various temperatures

	Carrier lifetime / ps	Built-in potential at liquid interface under equilibrium /eV	Series resistance / Ω	Surface recombination velocity / cm s^{-1}
500 °C	2.6	0.69	1200	10^{-4}
600 °C	3.0	0.77	1100	10^{-4}
700 °C	3.7	0.75	800	10^{-4}
800 °C	4.1	0.78	580	10^{-4}
900 °C	2.7	0.82	750	10^{-4}

Reference

1. J.-W. Jang, C. Du, Y. Ye, Y. Lin, X. Yao, J. Thorne, E. Liu, G. McMahon, J. Zhu, A. Javey, J. Guo and D. Wang, *Nat Commun*, 2015, **6**, 7447.
2. T. Minegishi, N. Nishimura, J. Kubota and K. Domen, *Chem. Sci.*, 2013, **4**, 1120-1124.
3. Y. Xiao, C. Feng, J. Fu, F. Wang, C. Li, V. F. Kunzelmann, C.-M. Jiang, M. Nakabayashi, N. Shibata, I. D. Sharp, K. Domen and Y. Li, *Nat. Catal.*, 2020, **3**, 932-940.
4. J. Liu, T. Hisatomi, G. Ma, A. Iwanaga, T. Minegishi, Y. Moriya, M. Katayama, J. Kubota and K. Domen, *Energy Environ. Sci.* , 2014, **7**, 2239-2242.
5. J. Liu, T. Hisatomi, M. Katayama, T. Minegishi, J. Kubota and K. Domen, *J. Mater. Chem. A*, 2016, **4**, 4848-4854.
6. https://refractiveindex.info/?shelf=main&book=Fe2O3&page=Querry-o.
7. B. Klahr, S. Gimenez, F. Fabregat-Santiago, T. Hamann and J. Bisquert, *J. Am. Chem. Soc.* , 2012, **134**, 4294-4302.
8. K. Sivula, F. Le Formal and M. Grätzel, *ChemSusChem*, 2011, **4**, 432-449.